IEEE Access
Multidisciplinary | Rapid Review | Open Access Journal

Received March 20, 2020, accepted April 9, 2020, date of publication April 13, 2020, date of current version April 28, 2020.

Digital Object Identifier 10.1109/ACCESS.2020.2987466

A Demodulation Model of Dynamic Low-Finesse Fabry-Perot Cavity Based on the Instantaneous Frequency

WEI ZHANG[1], BING XIONG[2], BIN SHAO[1], XIAOHUA LEI[1], AND WEIMIN CHEN[1]

[1]Key Laboratory for Optoelectronic Technology and Systems, Ministry of Education, College of Optoelectronic Engineering, Chongqing University, Chongqing 400044, China

[2]Science and Technology on Altitude Simulation Laboratory, AECC Sichuan Gas Turbine Establishment, Mianyang 621700, China

Corresponding authors: Wei Zhang (zhangwei1213052@cqu.edu.cn) and Weimin Chen (wmchen0802@126.com)

This work was supported in part by the National Natural Science Foundation of China under Grant 51805054 and Grant 51675068, in part by the China Postdoctoral Science Foundation under Grant 2018M643405, and in part by the Technology Innovation Platform Project of Aero Engine Corporation of China (AECC) under Grant SHYS-GXDPL-18.

ABSTRACT If the measurand changes during the spectrum acquisition process, it easily leads to the failure of the classic demodulation algorithms of low-finesse optical fiber Fabry-Perot (FP) sensors. To address this problem, a novel demodulation model is proposed based on the definition of the instantaneous frequency. The proposed model establishes the relationship between the optical path length (OPL) of the FP cavity and the instantaneous frequency distribution of the FP interference spectrum. The link between the classic FFT algorithm and this model is discussed, and it is found that this model can be viewed as a generalized form of the FFT algorithm. Based on this model, the Doppler-induced demodulation error is analyzed. The analysis uncovers that the average frequency of the FP interference spectrum should be used for the evaluation of the error, and the error is proportional to the variation of OPL during the spectrum acquisition period. Further, numerical simulation and an experiment were carried out to verify the proposed model, and results show that the proposed model is effective for the dynamic low-finesse FP cavity. It is the first time that the idea of instantaneous frequency is introduced for the FP demodulation, and this model provides us a new way to cope with the FP sensing signal.

INDEX TERMS Dynamic demodulation, Fabry-Perot, Doppler error, instantaneous frequency, Wigner-Ville distribution.

I. INTRODUCTION

Low-finesse optical fiber Fabry-Perot (FP) sensors are versatile, and they have been widely used for detecting various physical quantities, such as strain, temperature, pressure, vibration, and magnetic field [1]–[8]. These FP sensors have some differences in structure, but containing a low-finesse FP cavity is a key similarity for them. When utilized for measurement, the optical path length (OPL) of the FP cavity changes with the measurand, so demodulating the OPL (or the optical path difference, OPD) from the interference spectrum plays an important role in FP sensing applications [6].

For high-accuracy demodulation of low-finesse FP sensors, a variety of algorithms have been developed, such as phase algorithms (two [9], three [10], four [11] and five [12] wavelength techniques), FFT algorithm [13], [14] and its improved algorithms [1], [2], [15], DTG algorithm [9], wavelet phase extracting (WPE) algorithm [16], and Least-Squares fitting (LSF) [17] and its improved algorithms [18]. Yet, the models of the above-mentioned algorithms were all established on the static FP spectrum. In other words, the OPL of the FP cavity should be kept constant during the spectrum acquisition process. Otherwise, the famous Doppler phenomena [19] will distort the interference spectrum, leading to a big demodulation error, even demodulation failure. For this reason, these algorithms are only suitable for the measurement of the relative static measurand.

However, the dynamic measurement of physical quantities is very important in practices. For a dynamic measurand, the spectrum acquisition rate of an FP sensing system may not

The associate editor coordinating the review of this manuscript and approving it for publication was Zinan Wang.

be quick enough to keep the OPL of the FP cavity constant during the acquisition process. In this case, the OPL may vary irregularly during the spectrum acquisition process, and it is necessary to solve the demodulation problem of the relative dynamic FP cavity. To the best of our knowledge, little work has been reported to address this problem.

On the other hand, the idea of instantaneous frequency [20], [21] and time-frequency (TF) analysis methods [22], [23] have been widely used for non-stationary signal analysis. They were even applied to fiber Bragg grating sensing demodulation [24], but rarely to FP sensing demodulation.

In this paper, we propose a demodulation model for dynamic low-finesse FP cavity based on the definition of the instantaneous frequency. Using this model, the Doppler-induced demodulation error is analyzed. Moreover, the potential advantage of this model is demonstrated with both simulation and experimentation.

II. MODEL

Low-finesse optical fiber FP sensor means the finesse F of its reflection spectrum is much less than 1. In general, the low finesse is the result of the low reflectivity of the two surfaces forming the FP cavity. The low reflectivity makes the secondary reflections do not contribute much to the spectrum pattern of the interference spectrum. In fact, as long as one of the surfaces has low reflectivity, the secondary reflection can also be neglected [25]. Thus, the interference spectrum of a low-finesse FP cavity can be regarded as two-beam interference [3], [6], [8], [20], [25], and can be expressed as

$$I(k) = I_0 \{1 + \gamma \cos(2Lk + \varphi_0)\}, \ k \in [k_{\text{start}}, k_{\text{stop}}], \quad (1)$$

where I_0 is the power of the light source, k is the wavenumber defined by $k = 2\pi/\lambda$ (λ is the wavelength), γ is the fringe visibility, L is the OPL of FP cavity, φ_0 is the initial phase, k_{start} the wavenumber of the spectrum's first data point, and k_{stop} the wavenumber of the spectrum's last data point. After mean value removing and normalization, (1) can be rewritten as

$$I_{norm}(k) = \cos(2Lk + \varphi_0). \quad (2)$$

The $I_{norm}(k)$ is a cosine function with the variable k. Because the L is a constant, it can be demodulated accurately in the frequency domain of the spectrum with the widely-used FFT algorithm [14]. But if the L changes during the spectrum acquisition process, the variation of L should be taken into accounts. Thus, the L should be replaced by a function $L(k)$:

$$I_{norm}(k) = \cos\{2L(k)k + \varphi_0\}. \quad (3)$$

Supposing that the instantaneous frequency of $I_{\text{norm}}(k)$ is $f(k)$, and according to the definition of instantaneous frequency (the derivative of the phase [20]), we can obtain

$$f(k) = \frac{1}{2\pi}\frac{d[2L(k)k + \varphi_0]}{dk} = \frac{1}{\pi}\left[kL'(k) + L(k)\right]. \quad (4)$$

Equation (4) is a differential equation and its general solution is

$$L(k) = \frac{1}{k}\left[\int_{k_{\text{start}}}^{k} \pi f(k)\, dk + C\right], \quad (5)$$

where C is an arbitrary constant. To find the constant C, we assume that the $L(k)$ could be approximated by a m-th-order polynomial function of k in the range $[k_{\text{start}}, k_{\text{stop}}]$. Thus, the following equations can be obtained by taking m-th-order derivatives of (5) at $k = k_{\text{start}}$:

$$\begin{cases} \pi f(k_{\text{start}}) = k_{\text{start}} L'(k_{\text{start}}) + L(k_{\text{start}}), \\ \pi f'(k_{\text{start}}) = k_{\text{start}} L''(k_{\text{start}}) + 2L'(k_{\text{start}}), \\ \cdots \\ \pi f^{(m-1)}(k_{\text{start}}) = k_{\text{start}} L^{(m)}(k_{\text{start}}) + mL^{(m-1)}(k_{\text{start}}), \\ \pi f^{(m)}(k_{\text{start}}) = (m+1)\ L^{(m)}(k_{\text{start}}). \end{cases} \quad (6)$$

From (6), we can obtain the $L(k_{start})$:

$$L(k_{\text{start}}) = \pi \sum_{i=0}^{m} \frac{(-k_{\text{start}})^i}{(i+1)!} f^{(i)}(k_{\text{start}}). \quad (7)$$

Combing (5) and (7), we can find the C and rewrite $L(k)$ as

$$L(k) = \frac{\pi}{k}\left[\int_{k_{\text{start}}}^{k} f(k)\, dk + k_{\text{start}} \sum_{i=0}^{m} \frac{(-k_{\text{start}})^i}{(i+1)!} f^{(i)}(k_{\text{start}})\right]. \quad (8)$$

Because the $f^{(i)}(k_{\text{start}})$ can be calculated through the i-th-order derivative of the $f(k)$, the dynamic FP cavity could be demodulated if the $f(k)$ (or normalized $f_{norm}(k) = 2f(k)/f_s$, f_s is the sampling frequency of the spectrum) is known.

To calculate the $f(k)$, one can use different TF analysis methods such as short-time Fourier transform, wavelet transform, and Wigner-Ville distribution (WVD). In this paper, the WVD is selected because it gives the highest energy concentration in the TF plane and is a nonparametric technique [26], [27]. The WVD of the spectrum $I_{\text{norm}}(k)$ can be calculated with the following integral:

$$W[k,f] = \frac{1}{2\pi}\int z\left(k - \frac{1}{2}\tau\right) z^*\left(k + \frac{1}{2}\tau\right) e^{-j2\pi f(k)\tau} d\tau,$$
$$z(k) = I_{norm}(k) + j\mathbf{H}[I_{norm}(k)], \quad (9)$$

where $\mathbf{H}$ is the Hilbert transform. By polynomial fitting of the ridge line of $W[k,f]$, one can get the $f(k)$ (or $f_{norm}(k)$).

Because the model is derived from (1) which is actually an expression for two-beam interference, theoretically, it is not only effective for the low-finesse FP interferometer but also the Mach-Zenhder and Michelson interferometer.

III. DISCUSSION OF THE MODEL

A. RELATIONSHIP WITH THE FFT ALGORITHM

As mentioned above, the FFT demodulation algorithm estimates the L according to the frequency of the spectrum, and the proposed demodulation model is established on the instantaneous frequency of the spectrum. The modeling base

of the proposed model would make it more powerful than the FFT algorithm.

In fact, the FFT algorithm is just a special case of the proposed model. For the case of m = 0 (indicating the FP cavity remains still during the acquisition period of the spectrum), the $f(k)$ in (8) will become a constant which equals the frequency of the spectrum. Then, (8) can be reduced to

$$L(k)|_{m=0} = \pi f_{peak} = \frac{\pi f_{peak\_norm} f_s}{2} = \pi \frac{2 f_{peak\_norm}}{\Delta k}, \quad (10)$$

where f_{peak} and $f_{\text{peak\_norm}}$ are respectively the frequency and the normalized frequency of the spectrum, and k is the spectral sampling interval. Traditionally, the f_{peak} is obtained by finding the peak frequency in the frequency domain, and this is exactly what the FFT method does. So, the demodulation formula of the widely-used FFT algorithm [14] is the same as (10). Obviously, the proposed demodulation model could be seen as a generalized form of the FFT demodulation algorithm.

B. SCOPE OF APPLICATION

For the successful application of this model to the demodulation of a dynamic FP cavity, one needs to understand its usage condition. First, the obtained FP spectrum must satisfy the Nyquist sampling theorem, i.e., the condition $f_{norm}(k) < 1$ must be guaranteed. Besides, as we usually take the positive frequency domain when doing the TF analysis, the $f_{norm}(k)$ should be larger than 0. Thereby, the performance space of this model is limited to

$$0 < f_{norm}(k) < 1. \quad (11)$$

Theoretically, this model works as long as the condition (11) is satisfied.

IV. DISCUSSION OF DOPPLER-INDUCED DEMODULATION ERROR

When the OPL changes during the spectrum acquisition process, it will cause the famous Doppler phenomenon, resulting in a Doppler-induced demodulation error. From the view of the frequency domain, the Doppler-induced error has been discussed in reference [19]. Based on our model, we are going to discuss it from the perspective of the wavenumber-frequency domain.

In the range of $[k_{\text{start}}, k_{\text{stop}}]$, the average value of $f_{norm}(k)$ can be calculated by

$$\begin{aligned} f_{avg} &= \frac{\int_{k_{start}}^{k_{stop}} f_{norm}(k)dk}{k_{stop}-k_{start}} = \frac{2}{f_s}\frac{\int_{k_{start}}^{k_{stop}} \frac{1}{\pi}\left[kL'(k)+L(k)\right]dk}{k_{stop}-k_{start}} \\ &= \frac{2}{\pi f_s}\left\{L\left(k_{stop}\right)+\frac{k_{start}}{k_{stop}-k_{start}}\left[L\left(k_{stop}\right)-L\left(k_{start}\right)\right]\right\} \\ &= \frac{2}{\pi f_s}\left\{L\left(k_{stop}\right)+\frac{k_{start}}{k_{stop}-k_{start}}\Delta L\right\}, \end{aligned} \quad (12)$$

where ΔL is the variation of the OPL during the spectrum acquisition period. If one uses the f_{avg} to demodulate the OPL, he will get

$$L_{avg} = \frac{\pi f_s}{2} f_{avg} = L\left(k_{stop}\right) + \frac{k_{start}}{k_{stop}-k_{start}}\Delta L. \quad (13)$$

Obviously, the demodulation error R of the L_{avg} is

$$R = \frac{k_{start}}{k_{stop}-k_{start}}\Delta L. \quad (14)$$

From (14), it can be seen that the Doppler-induced demodulation error is determined by ΔL, and this is valid for all the cases of m $\geqslant$ 1. For the special case of m = 1, if we assume OPL changes with a constant velocity v during the spectrum acquisition period Δt, the demodulation error can be rewritten as

$$R|_{m=0} = \frac{k_{start}}{k_{stop}-k_{start}} v\Delta t = \frac{f_{start}}{f_{stop}-f_{start}} v\Delta t, \quad (15)$$

where f_{start} and f_{stop} are respectively the light frequencies of the interference spectrum's first and last data points. The reference [19] also gave a Doppler-induced demodulation error formula as follows

$$R_{ref} = -\frac{f_0}{\Delta f_0} v\Delta t, \quad (16)$$

where f_0 is the center frequency of the light source, and f_0 is the frequency range of the light source. For example, for a commonly-used broadband light source with a wavelength range of 1529nm$\sim$1569nm, we have f_{start} = 196207GHz, f_{stop} = 191205GHz, f_0 = 193673GHz, and f_0 = 5002GHz. Then, one can find $R|_{\text{m=0}}$ is almost the same as R_{ref} ($R|_{\text{m=0}} \approx 1.01R_{\text{ref}}$). In other words, (15) (or (16)) is just a special case of (14). From the wavenumber-frequency domain, one can better understand the Doppler-induced error.

In addition, it should be emphasized that, the f_{avg} is calculated through the $f_{norm}(k)$ and different from the peak frequency f_{peak} determined by the FFT algorithm. So, the demodulation error of the FFT algorithm does not have such an exact relationship shown by (14). But in some cases where f_{peak} approximates f_{avg}, the demodulation error of FFT can be approximated by (14). In fact, understanding the influence of the dynamic FP cavity on the demodulation error of the FFT algorithm is of great importance. Because, for other FP demodulation algorithms, such as DTG [9], WPE [16], and LSF [17], the FFT is used in the first step to make a rough estimate of the OPL, then more accurate OPL is searched around the estimated value. Generally, the search range is less than a few microns, but the Doppler-induced error of FFT easily goes far out of this range. In other words, if the FFT algorithm gets a wrong estimation of OPL, these reported FP demodulation algorithms will probably fail. Considering the importance of the FFT algorithm, we will compare its demodulation result with the L_{avg} in our following discussions.

V. SIMULATION

In this section, some simulation interference spectra are introduced to validate the demodulation model and the analysis of demodulation error. These spectra are simulated with the

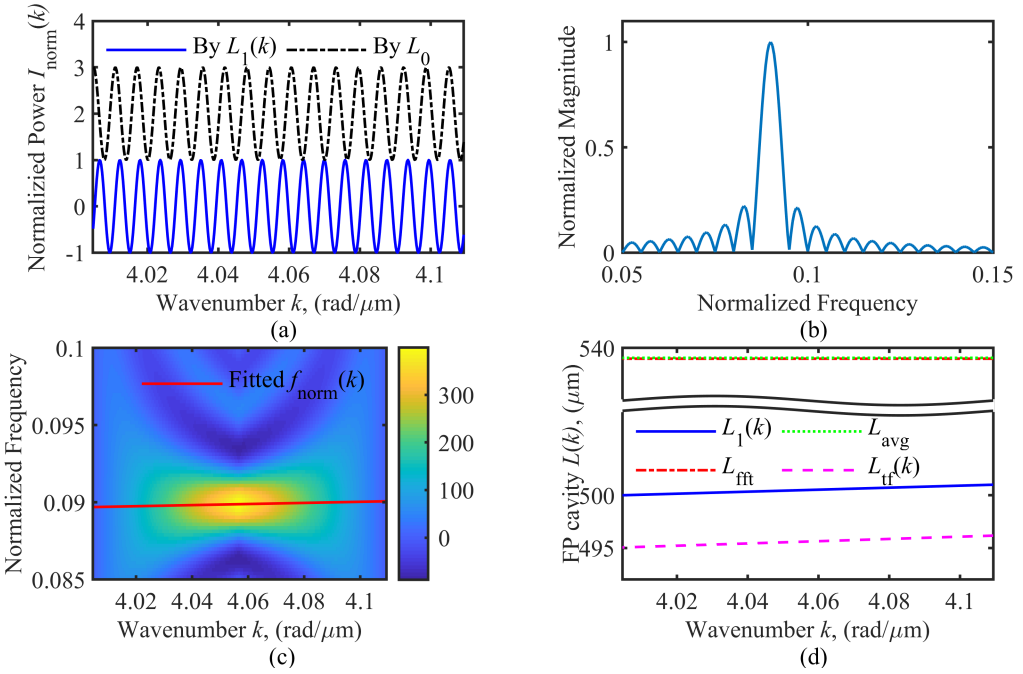

FIGURE 1. (a) A comparison between a spectrum of dynamic FP cavity with $L_1(k)$ and a spectrum of static FP cavity with L_0 (the spectrum of L_0 is deliberately moved up to make it distinguishable from that of $L_1(k)$), (b) frequency spectrum of the dynamic spectrum, (c) the WVD of the dynamic spectrum and the fitted $f_{norm}(k)$, (d) theoretical FP cavity, and FP cavity demodulated by FFT algorithm, average frequency, and the proposed method.

same k_{start}, k_{stop}, and k ($k_{\text{start}} = 2\pi/1.569$ (rad/μm), $k_{\text{stop}} = 2\pi/1.529$ (rad/μm), $k = (k_{\text{stop}}\text{-}k_{\text{start}})/400$ (rad/μm)).

First, we let $L_1(k) = 500 + (k\text{-}k_{\text{start}})/(k_{\text{stop}}\text{-}k_{\text{start}})$ (μm) and generate an interference spectrum as shown in Fig.1(a). Meanwhile, a spectrum of a static FP cavity with the OPL $L_0 = 500\mu$m is plotted in Fig.1(a) for comparison. Because the expansion of OPL is only 1μm over the spectral range, the dynamic spectrum does not look much different from the static spectrum. In fact, the expansion of OPL just causes an increase from 17 to 18 in the fringes of the spectrum, and it is hard for one to distinguish whether or not such a spectrum is from a dynamic FP cavity. Further, we plot the frequency spectrum of the dynamic spectrum in Fig.1(b) and find it is still a single peak. In other words, one cannot notice anything unusual from the frequency domain as well. However, the demodulation error of FFT (see the L_{fft} Fig.1(d)) reaches about 38μm. Here, one may find the L_{fft} is almost the same with L_{avg}, and this is because the average frequency happens to approximate to the peak frequency. In our simulation, as $k_{\text{start}}/(k_{\text{stop}}\text{-}k_{\text{start}})$ equals 38 and the variation of the OPL is 1μm, the theoretical error of L_{avg} should be 38μm. As expected, the calculated L_{avg} in Fig.1(d) deviates from the $L_1(k_{\text{stop}})$ by 38μm, which agrees well with the theoretical prediction.

Then, the proposed demodulation method is applied to the dynamic interference spectrum. To improve the frequency resolution of the WVD, the spectrum is extended by zero-padding (the padding length is 10 times the length of the spectrum). Fig.1(c) gives the $W[k, f]$, the wavenumber-frequency domain of the spectrum, and the linear fitting of the ridge line of $W[k, f]$. Though it is hard for software even a man to perceive the existence of the Doppler error from the frequency domain, it becomes easy in the wavenumber-frequency domain as the $f_{norm}(k)$ is obviously not a constant. Moreover, using the fitted $f_{norm}(k)$, we can reduce the error and get a more calculate cavity. The calculated dynamic FP cavity $L_{\text{tf}}(k)$ is plotted in Fig.1(d). From Fig.1(d), we can see that the demodulation error of the proposed method is about 5μm, which makes a great improvement comparing to the FFT algorithm.

To further investigate the effect of noise on the proposed method, white Gaussian noises with different SNRs are added to the dynamic spectrum. A total set of 30 spectra for each SNR level are generated to determine the demodulation error. The demodulation error shown in Fig.3 is the mean value of $|\max[L_{\text{tf}}(k)\text{-}L_1(k)]|$, and the error bar is the standard deviation of $|\max[L_{\text{tf}}(k)\text{-}L_1(k)]|$. It can be seen from Fig.2 that the proposed model has a relatively good performance under the condition of SNR$\geq$30dB. In most situations, the SNR of an FP interference spectrum can be higher than 30dB.

To further validate the application scope of the proposed model, two extreme dynamic FP cavities with $L_2(k) = 500 - 12(k\text{-}k_{\text{start}})/(k_{\text{stop}}\text{-}k_{\text{start}})$ (μm) and$L_3(k) = 500 + 135(k\text{-}k_{\text{start}})/(k_{\text{stop}}\text{-}k_{\text{start}})$ (μm) are employed to generate the interference spectra, and corresponding spectra with SNR = 30dB are plotted in Fig.3(a) and Fig.4(a). In these extreme conditions, traditional FP demodulation algorithms are difficult to perform. For example, at least two peaks

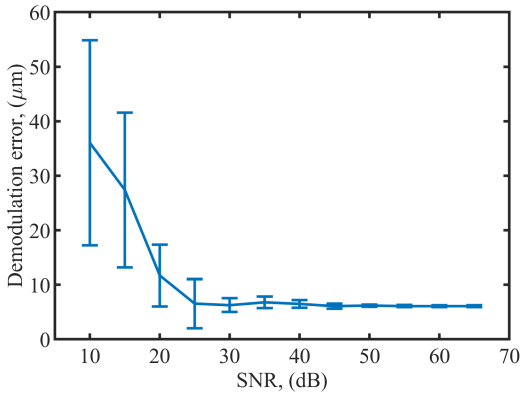

FIGURE 2. Effect of noise on the demodulation error of the proposed method.

are needed for the phase algorithms, but the interference spectrum in Fig.3(a) has only one peak. The frequency spectrum in Fig.4(b) is obviously abnormal, which frustrates these FFT-based FP demodulation algorithms. Although these extreme cases are rare in practices, they can demonstrate the advantage of the proposed model.

Because the L of $L_2(k)$ and $L_3(k)$ are respectively -12μm and 135μm, corresponding theoretical errors of L_{avg} should be about -458μm and 5160μm. As can be seen from Fig.3(d) and Fig.4(d) that, the deviations of L_{avg}s from $L_2(k_{\text{stop}})$ and $L_3(k_{\text{stop}})$ are -461μm and 5159μm, respectively. The slight difference between the theoretical and simulation errors are mainly due to the calculation deviation of $f_{\text{norm}}(k)$. For the L_{fft} shown in the Fig.3(d), its error approximates to the error of L_{avg}, and this is because the frequency spectrum (see Fig.3(b)) still does not have enough distortion. But for the L_{fft} in Fig.4(d), it deviates obviously from L_{avg}, and this is due to the serious distortion of the frequency spectrum (see Fig.4(b)). By the comparison of L_{fft} and L_{avg}, it can be concluded that f_{avg} is more suitable for the evaluation of the Doppler-induced demodulation error than the f_{peak}.

From Fig.3(c) and Fig.4(c), one can find that the normalized instantaneous frequency $f_{\text{norm}}(k)$ approaches respectively the lower and upper limits. Even so, the proposed algorithm still stays a high demodulation accuracy (see $L_{\text{tf}}(k)$s in Fig.3(d) and Fig.4(d)). Under the occasions of the large variation of OPL, the proposed method exhibits more obvious advantages over the traditional FP algorithms.

Theoretically, the proposed model is effective even when the variation of OPL is not linear. We tried some cases of non-linear changing OPL, but the demodulation accuracy is not as high as the linear cases. For a non-linear changing OPL, its interference spectrum becomes a non-linear chirped signal. For a non-linear chirped signal, the accuracy of $f_{norm}(k)$ calculated by the WVD will decline, and this is because the kernel of WVD is a function reconstructed from the central finite difference estimator [28]. In fact, the accurate calculation of $f_{norm}(k)$ is the core of the success of the proposed model, and the accuracy of $f_{norm}(k)$ relies entirely on the TF analysis method adopted. For the WVD, its kernel limits it to the linear cases, so it has to be replaced by a more powerful TF analysis method to adapt to nonlinear cases. In theory, to ensure the accuracy of $f_{norm}(k)$ for nonlinear cases, the kernel

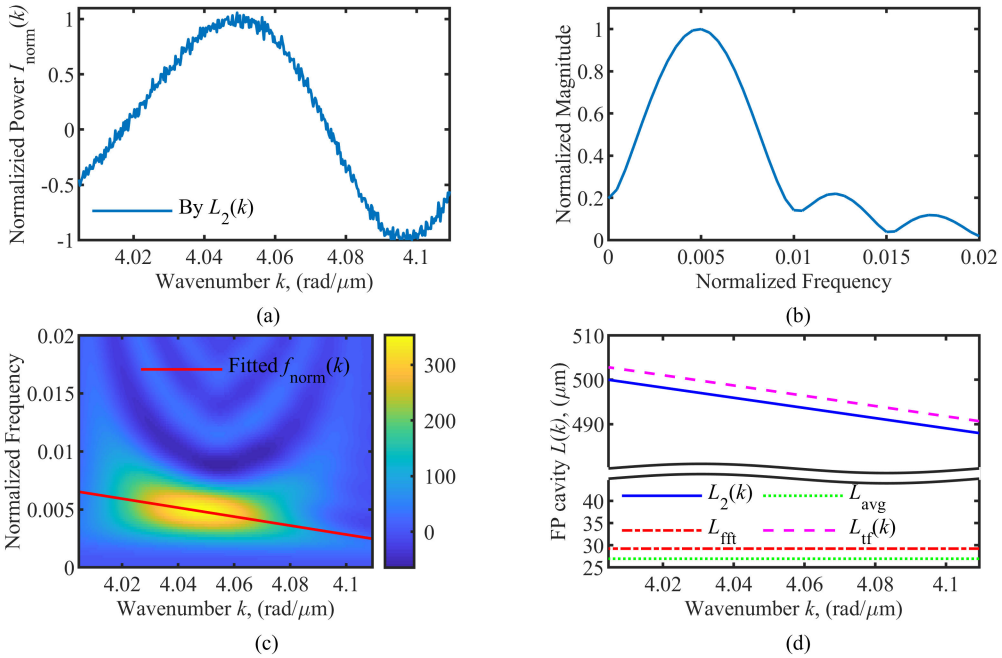

FIGURE 3. (a) A spectrum of a dynamic FP cavity with $L_2(k)$ (SNR = 30dB), (b) frequency spectrum of the dynamic spectrum, (c) the WVD of the dynamic spectrum and the fitted $f_{norm}(k)$, (d) theoretical FP cavity, and FP cavity demodulated by FFT algorithm, average frequency, and the proposed method.

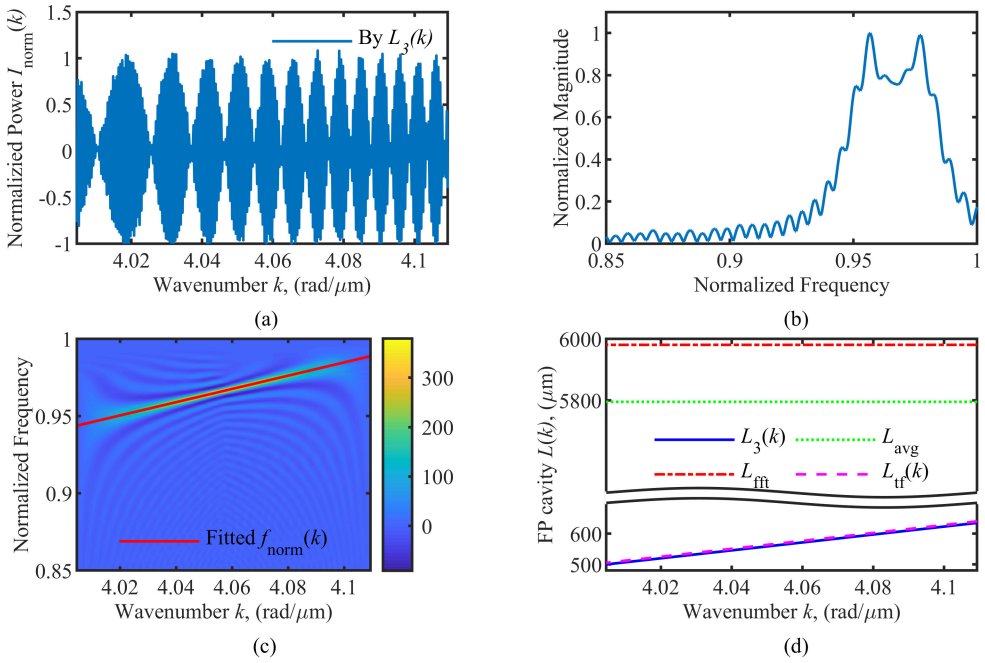

FIGURE 4. (a) A spectrum of dynamic FP cavity with $L_3(k)$ (SNR = 30dB), (b) frequency spectrum of the dynamic spectrum, (c) the WVD of the dynamic spectrum and the fitted $f_{norm}(k)$, (d) theoretical FP cavity, and FP cavity demodulated by FFT algorithm, average frequency, and the proposed method.

of the TF analysis method should have a non-linear form similar to the real instantaneous frequency of the interference spectrum. From the kernel's view, some parametric TF analysis methods, such as polynomial WVD [28], and polynomial chirplet transform [23], may have potentials to address the problem of non-linear cases. But determining the parameters of these methods suitable for arbitrary non-linear cases is not easy. We are going to further study it in our future work.

VI. EXPERIMENT

To experimentally verify the effectiveness of the proposed demodulation model, we constructed a system as shown in Fig.5 to measure the interference spectrum of a linear changing FP cavity. The waveform generator (DG4102, RIGOL) provides a sawtooth voltage signal, and the signal is amplified by the amplifier (HAS 4011, NF Corporation) and applied to the PZT (PK4FTH3P2, Thorlabs). Thus, a dynamic FP cavity is formed between the end-face of the optical fiber and the aluminum reflective surface bonded on the PZT. Because the reflectivity of the end-face of optical fiber is about 0.04, this cavity is a low-finesse FP cavity (the finesse $F \ll 1$ according to its calculation formula $F = \pi(r_1 r_2)\text{^}(0.5)/(1\text{-}r_1 r_2)$, where r_1 and r_2 are the reflectivities of FP cavity boundaries). An optical spectrum analyzer (made by Gaussian optics photoelectric technology co. ltd, China) and a coupler are used to measure the FP interference spectrum. The optical spectrum analyzer is mainly composed of a tunable laser and a photodetector, and its spectral resolution is 10 pm, and it takes 0.4s

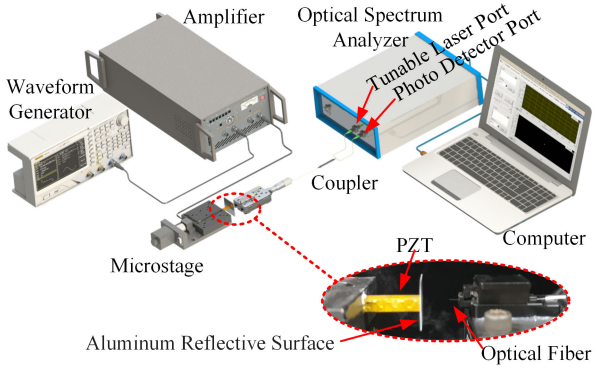

FIGURE 5. Experimental setup for the spectrum measurement of dynamic FP cavity.

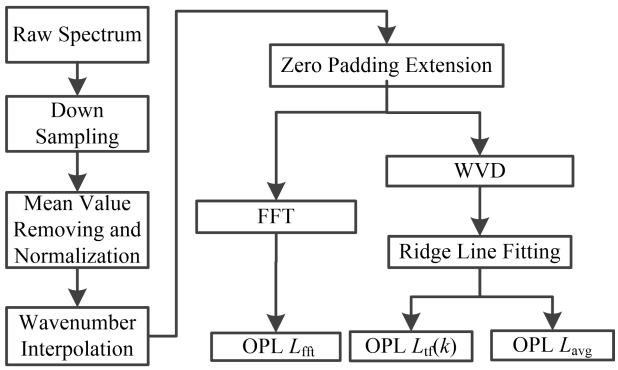

FIGURE 6. Demodulation flow chart of FFT algorithm, average frequency and the proposed model for the experimentally measured spectrum.

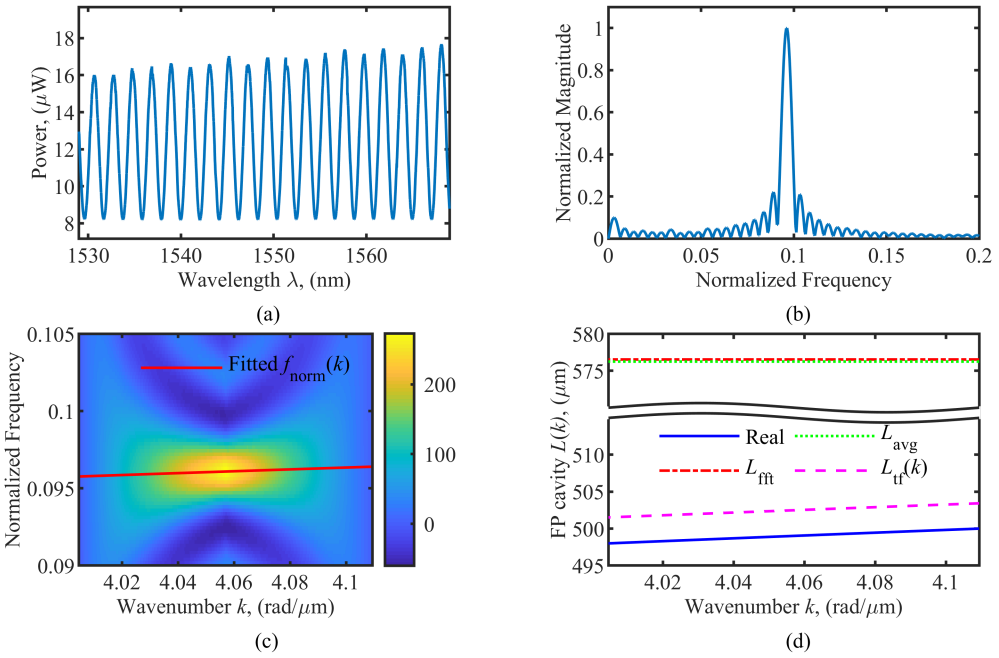

FIGURE 7. (a) An experimental spectrum of dynamic FP cavity (500μm FP cavity with 2μm displacement during the spectrum measurement), (b) frequency spectrum of the dynamic spectrum, (c) the WVD of the dynamic spectrum and the fitted $f_{norm}(k)$, (d) theoretical FP cavity, and FP cavity demodulated by FFT algorithm, average frequency, and the proposed method.

to sweep over a range of 40nm (1529∼1569nm). During the experiment, the initial OPL L_0 is adjusted to 500μm by the cooperation of the micro stage and an online demodulation software of static FP cavity developed by ourselves (the resolution of our software is 10 pm). Besides, we use a laser vibrometer (OFV-5000, Polytec) to calibrate the dynamic displacement provided by the PZT, and the displacement resolution is 0.1 pm.

The demodulation process of the experimentally measured spectrum is illustrated in Fig.6. As the sampling of the raw spectrum as shown in Fig.7(a) is relatively dense, down sampling is applied to the spectrum to reduce the calculation amount. The down sampling is acceptable as long as the sampling law is satisfied. In this paper, the sample rate of the spectrum is decreased by a factor of 10. In turn, the mean value removing and the normalization are applied to the downsampled spectrum. Because the measured spectrum is uniformly sampled in the wavelength domain, it needs to transform the spectrum to the wavenumber domain by the interpolation. Here, the spline interpolation is used. Afterward, we extend the spectrum by zero-padding to increase the frequency resolution of the WVD and the FFT (the padding length is 10 times the length of the downsampled spectrum). Finally, the FFT algorithm, average frequency and the proposed method are respectively used to obtain L_{fft}, L_{avg} and $L_{\text{tf}}(k)$.

Fig.7(b) shows the frequency spectrum of the experimental dynamic spectrum. As can be seen that it is a standard peak, which seems like one without Doppler error. But from the wavenumber-frequency domain as shown in Fig.7(c), it is easy to realize that there will be an error if those reported algorithms are used. Fig.7(d) shows the comparison of L_{fft}, L_{avg}, and $L_{\text{tf}}(k)$. For L_{avg}, it deviates from the real cavity by about 76μm, and this is because there is a 2μm displacement during the spectrum measurement. Given the proximity between the average frequency and peak frequency of such a dynamic spectrum, L_{fft} is almost the same as L_{avg}. In contrast, the demodulation error of $L_{\text{tf}}(k)$ is only 4μm, much smaller than that of the FFT algorithm. More importantly, the $L_{\text{tf}}(k)$ reconstructs the changing trend of the dynamic FP cavity. In addition, though there is a small difference between the real low-finesse FP spectrum and the two-beam interference spectrum [29], the experimental result confirms the effectiveness of this model for the low-finesse FP cavity.

VII. CONCLUSION

In summary, a novel demodulation model for the dynamic FP cavity is presented by introducing the instantaneous frequency. To some extent, this model can be viewed as a generalized form of the classical FFT demodulation algorithm, but it is more powerful.

First, this model gives us a new perspective on the FP interference spectrum from the wavenumber-frequency domain. When applying a traditional FP demodulation algorithm to a dynamic spectrum, it is probably difficult to notice the Doppler-induced error from the wavenumber or frequency domain, but it becomes simple in the wavenumber-frequency domain. From the view of instantaneous frequency, the

theoretical Doppler-induced error is derived, and the variation of OPL during the spectrum acquisition period is found to be the determinant of the error. Besides, we suggest that the average frequency should be used for the evaluation of the error despite that the peak frequency is close to the average frequency in some cases.

Second, the model provides us a new way of demodulating dynamic FP cavity only by the use of the interference spectrum. For most reported algorithms, the FFT algorithm is their base or first step, but unfortunately, the dynamic FP cavity has great impacts on the FFT algorithm. By the simulation and experiment, the model has been proven to be promising for the demodulation of the dynamic FP cavity. Although only linear cases are used to demonstrate the effectiveness of the model, this model is theoretically applicable to nonlinear cases as long as the accurate instantaneous frequency distribution can be obtained. The WVD adopted in the paper does not perform well for nonlinear cases, but a more advanced TF analysis method has the potential to cope with it and finding such a method is our future work.

REFERENCES

[1] Z. H. Yu and A. B. Wang, "Fast white light interferometry demodulation algorithm for low-finesse Fabry–Pérot sensors," *IEEE Photon. Technol. Lett.*, vol. 27, no. 8, pp. 817–820, Apr. 15, 2015.

[2] K. Chen, Z. H. Yu, Q. X. Yu, M. Guo, Z. H. Zhao, C. Qu, Z. F. Gong, and Y. Yang, "Fast demodulated white-light interferometry-based fiber-optic Fabry–Pérot cantilever microphone," *Opt. Lett.*, vol. 43, no. 14, pp. 3417–3420, Jul. 2018.

[3] M. Islam, M. Ali, M.-H. Lai, K.-S. Lim, and H. Ahmad, "Chronology of Fabry–Pérot interferometer fiber-optic sensors and their applications: A review," *Sensors*, vol. 14, no. 4, pp. 7451–7488, 2014.

[4] A. Zhou, B. Y. Qin, Z. Zhu, Y. X. Zhang, Z. H. Liu, J. Yang, and L. B. Yuan, "Hybrid structured fiber-optic Fabry–Pérot interferometer for simultaneous measurement of strain and temperature," *Opt. Lett.*, vol. 39, no. 18, pp. 5267–5270, Jul. 2014.

[5] M. D. Tamin and J. Meyer, "Quasi-distributed Fabry–Pérot optical fibre sensor for temperature measurements," *IEEE Access*, vol. 6, pp. 66235–66242, 2018.

[6] J. T. G. Bonilla, H. G. Bonilla, V. M. R. Betancourtt, M. E. S. Morales, J. R. Gomes, A. C. Zamora, and A. C. Bonilla, "Low-finesse Fabry–Pérot interferometers applied in the study of the relation between the optical path difference and poles location," *Sensors*, vol. 20, no. 2, p. 453, Jan. 2020.

[7] E. Kendir and Ş. Yaltkaya, "Variations of magnetic field measurement with an extrinsic Fabry–Pérot interferometer by double-beam technique," *Measurement*, vol. 151, Feb. 2020, Art. no. 107217.

[8] Y. Wu, L. Xia, W. Li, and J. Xia, "Highly sensitive Fabry–Pérot demodulation based on coarse wavelength sampling and Vernier effect," *IEEE Photon. Technol. Lett.*, vol. 31, no. 6, pp. 487–490, Mar. 15, 2019.

[9] S. M. Musa, "Real-time signal processing and hardware development for a wavelength modulated optical fiber sensor system," Ph.D. dissertation, Dept. ECPE, Virginia Tech., Blacksburg, VA, USA, 1997.

[10] J. M. Kilpatrick, W. N. MacPherson, J. S. Barton, and J. D. C. Jones, "Phase-demodulation error of a fiber-optic Fabry–Pérot sensor with complex reflection coefficients," *Appl. Opt.*, vol. 39, no. 9, p. 1382, Mar. 2000.

[11] A. Ezbiri and R. P. Tatam, "Interrogation of low finesse optical fibre Fabry–Pérot interferometers using a four wavelength technique," *Meas. Sci. Technol.*, vol. 7, no. 2, pp. 117–120, Feb. 1996.

[12] A. Ezbiri and R. P. Tatam, "Five wavelength interrogation technique for miniature fibre optic Fabry–Pérot sensors," *Opt. Commun.*, vol. 133, nos. 1–6, pp. 62–66, Jan. 1997.

[13] H. Y. Choi, K. S. Park, S. J. Park, U.-C. Paek, B. H. Lee, and E. S. Choi, "Miniature fiber-optic high temperature sensor based on a hybrid structured Fabry–Pérot interferometer," *Opt. Lett.*, vol. 33, no. 21, p. 2455, Nov. 2008.

[14] C. Ma and A. B. Wang, "Signal processing of white-light interferometric low-finesse fiber-optic Fabry–Pérot sensors," *Appl. Opt.*, vol. 52, no. 2, pp. 127–138, Jan. 2013.

[15] Z. Yu and A. Wang, "Fast demodulation algorithm for multiplexed low-finesse Fabry–Pérot interferometers," *J. Lightw. Technol.*, vol. 34, no. 3, pp. 1015–1019, Feb. 1, 2016.

[16] B. Zhang, X. Tong, P. Hu, Q. Guo, Z. Zheng, and C. Zhou, "Wavelet phase extracting demodulation algorithm based on scale factor for optical fiber Fabry–Pérot sensing," *Opt. Express*, vol. 24, no. 26, p. 29506, Dec. 2016.

[17] Y. Wu, L. Xia, N. Cai, and L. Zhu, "A highly precise demodulation method for fiber Fabry–Pérot cavity through spectrum reconstruction," *IEEE Photon. Technol. Lett.*, vol. 30, no. 5, pp. 435–438, Mar. 1, 2018.

[18] X. W. Gui, M. A. Galle, L. Qian, W. L. Liang, C. M. Zhou, Y. W. Ou, and D. Fan, "Demodulation method combining virtual reference interferometry and minimum mean square error for fiber-optic Fabry–Pérot sensors," *Chin. Opt. Lett.*, vol. 16, no. 1, Jan. 2018, Art. no. 010606.

[19] E. A. Moro, M. D. Todd, and A. D. Puckett, "Understanding the effects of Doppler phenomena in white light Fabry–Pérot interferometers for simultaneous position and velocity measurement," *Appl. Opt.*, vol. 51, no. 27, pp. 6518–6527, Sep. 2012.

[20] P. J. Loughlin, "What are the time-frequency moments of a signal?" *Proc. SPIE*, vol. 4474, Nov. 2001, pp. 35–44.

[21] L. Stanković, I. Djurović, S. Stanković, M. Simeunović, S. Djukanović, and M. Daković, "Instantaneous frequency in time–frequency analysis: Enhanced concepts and performance of estimation algorithms," *Digit. Signal Process.*, vol. 35, pp. 1–13, Sep. 2014.

[22] Y.-L. Sheu, H.-T. Wu, and L.-Y. Hsu, "Exploring laser-driven quantum phenomena from a time-frequency analysis perspective: A comprehensive study," *Opt. Express*, vol. 23, no. 23, p. 30459, Nov. 2015.

[23] P. Zhou, Z. K. Peng, S. Q. Chen, Y. Yang, and W. M. Zhang, "Non-stationary signal analysis based on general parameterized time–frequency transform and its application in the feature extraction of a rotary machine," *Frontiers Mech. Eng.*, vol. 13, no. 2, pp. 292–300, Feb. 2018.

[24] J. Azana, M. A. Muriel, L. R. Chen, and P. W. E. Smith, "Fiber Bragg grating period reconstruction using time-frequency signal analysis and application to distributed sensing," *J. Lightw. Technol.*, vol. 19, no. 5, pp. 646–654, May 2001.

[25] C. Ma, "Modeling and signal processing of low-finesse Fabry–Pérot interferometric fiber optic sensors," Ph.D. dissertation, Dept. ECPE, Virginia Tech., Blacksburg, VA, USA, 2012.

[26] L. Cohen, "Time-frequency distributions–A review," *Proc. IEEE*, vol. 77, no. 7, pp. 941–981, Jul. 1989.

[27] J. Xu, L. Durand, and P. Pibarot, "Nonlinear transient chirp signal modeling of the aortic and pulmonary components of the second heart sound," *IEEE Trans. Biomed. Eng.*, vol. 47, no. 10, pp. 1328–1335, Oct. 2000.

[28] B. Boashash and P. O'Shea, "Polynomial Wigner-Ville distributions and their relationship to time-varying higher order spectra," *IEEE Trans. Signal Process.*, vol. 42, no. 1, pp. 216–220, Jan. 1994.

[29] J. L. Santos, A. P. Leite, and D. A. Jackson, "Optical fiber sensing with a low-finesse Fabry–Pérot cavity," *Appl. Opt.*, vol. 31, no. 34, pp. 7361–7366, Dec. 1992.

WEI ZHANG received the B.S. degree in measurement technology and instrumentation and the Ph.D. degree in instrument science and technology from Chongqing University, China, in 2012 and 2016, respectively.

He holds a Postdoctoral position with the College of Optoelectronic Engineering, Chongqing University. His current research interests include optical fiber sensors, optical sensing systems, laser /microwave radar, and signal processing.

BING XIONG received the M.S. degree in aerospace propulsion theory and engineering from the Chinese Aeronautical Establishment, in 2009.

He is currently a Researcher with AECC Sichuan Gas Turbine Establishment, China. His main research interest includes aeronautic testing.

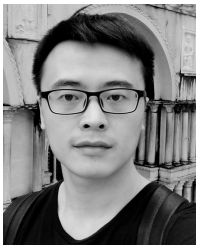

BIN SHAO received the B.S. degree from Chongqing University, China, in 2014, where he is currently pursuing the Ph.D. degree in optical engineering.

His current research interest includes optical fiber sensing systems.

XIAOHUA LEI received the Ph.D. degree from Chongqing University, Chongqing, China, in 2008.

She is currently an Associate Professor with the College of Optoelectronic Engineering, Chongqing University. Her research interests include optical fiber sensing technology and signal processing.

WEIMIN CHEN received the B.S. degree in optical instruments and engineering from Zhejiang University, China, in 1982, and the M.S. degree in precision instrument and machinery and the Ph.D. degree in instrument science and technology from Chongqing University, China, in 1988 and 1999, respectively.

From 1991 to 1992, he was a Visiting Scholar with the Tokyo University of Agriculture and Technology, Japan. He is currently a Professor and the Vice Director of the Key Laboratory for Optoelectronic Technology and Systems, Ministry of Education, Chongqing University. He is the author or coauthor of more than 500 journal articles. His research interests include sensors, precision measurement technology, photoelectric technology, and smart structures and systems. He is a member of SPIE and the Executive Director of the Chinese Optical Society.